Experimental Violation of a Leggett-Garg inequality with macroscopic crystals

Zong-Quan Zhou,[1] Susana F. Huelga*,[2] Chuan-Feng Li†,[1] and Guang-Can Guo[1]

[1]*Key Laboratory of Quantum Information, University of Science and Technology of China, CAS, Hefei, 230026, China*

[2]*Institut für Theoretische Physik, Albert-Einstein-Allee 11, Universität Ulm, D-89069 Ulm, Germany*

(Dated: September 12, 2012)

Abstract

The quantum mechanical description of the world leads to predictions that defy our daily experience when dealing with macroscopic objects. Schrödinger's famous *cat* illustrates most graphically the paradoxical situations that one encounters when extrapolating the quantum rules to systems possessing macroscopically distinguishable states. Leggett and Garg formulated this question qualitatively by deriving a series of inequalities based upon the premises of macroscopic realism [1, 2] which have been recently tested within several microscopic systems [3–7] and micrometer-sized superconducting circuits [8]. Here we present an experimental violation of Legget-Garg inequalities (LGI) with millimeter-sized crystals whose state can be thought of as a *cat of cats*. Through the reversible transfer of polarization state of single photons and the collective excitation states of crystals, we prepared superposition states of two macroscopic crystals separated by a distance in the mm range. The phase relation between the states in the superposition is governed by the dynamics of a large number of individual atoms and can be controlled with a frequency detuned and polarization dependent atomic frequency comb [9–13]. The quantum character of the considered global state is therefore governed by a macroscopic quantity, which allows for an additional level of complexity in the system. The observed violation of a LGI confirms the persistence of quantum coherence effects within macroscopic objects which can be seen with a naked eye.

PACS numbers:

* email:susana.huelga@uni-ulm.de

† email:cfli@ustc.edu.cn

Ever since the birth of quantum mechanics (QM) it has been stressed the difficulty to reconcile the behavior of quantum particles and our intuitive experience when dealing with macroscopic objects, which should occupy definite states at all times and independently of the observers. Some physicists, with Niels Bohr as a precursor, argued that the solution to this problem requires dividing the world into a microscopic domain described by the quantum formalism and the macroscopic level of measuring apparatus, which is postulated to behave classically. However, this division unavoidably carries a degree of arbitrariness, as illustrated by the famous Schrödinger cat gedanken experiment [14], where the superposition state of an atom is shown to be transferable, in principle, to a superposition state of two macrocopically distinct states.

Following the argument presented in the 1935 Einstein-Podolsky-Rosen seminal paper [15], Bell derived an experimentally testable inequality, in which the premises of local realism yield statistical predictions that disagree with those of quantum mechanics [16]. Numerous experiments have confirmed the validity of the QM predictions in spatially separated microscopic systems, with various loop-holes regarding experimental deficiencies having been closed individually [17–19]. A loophole-free experimental violation of Bell inequality would lead to the sacrifice of either the locality or the realism assumption. On the other hand, in contexts where locality is not relevant, the focus is on the realism assumption at a level much closer to our everyday perception. Unlike the Bell inequality, which involves statistical correlations between states of two spatially separated systems, LGI are concerned with the correlations of the state of a single system at different times (autocorrelations) [1]. Introduced as the Bell inequalities in time, the violation of LGI excludes a hidden-variable description based upon the assumptions of macroscopic realism (a macroscopic system must at any time be in a definite one of its macroscopically distinct states) and the possibility to perform noninvasive measurements (measurements do not influence the actual state or the subsequent system dynamics of the system). LGI therefore provide a criterion to characterize the boundary between the quantum and the classical domains and could witness the persistence of coherence effects beyond the closed systems paradigm [20]. Testing the validity of standard quantum theory over larger and larger scales and increasing levels of complexity is important for assessing the relevance of genuinely quantum traits beyond microscopic scales [21] as well as analyzing the feasibility of unconventional decoherence models like those invoking spontaneous wave function collapse [22–25].

Until now, the experimental violation of LGI has been performed with microscopic objects, such as photons [3, 4], electron or nuclear spins [5–7] and the micrometer-sized superconducting 'transmon' system [8]. In practice, the main experimental challenge comes from the implementation of truly non-invasive measurements. However, the use of weak measurements [8] and schemes involving ancillary systems [7] have recently allowed for the first experimental results in the microscopic domain. To avoid the need of performing measurements at intermediate times, as required in the original formulation of the inequalities, it has been suggested that the condition of noninvasive measurements can be replaced by the weaker assumption of stationary correlations [26, 27]. The resulting formulation is then easily testable by using projective measurements. Within this framework, inequalities are derived from the premises of:

1) Macroscopic realism: A macroscopic object which has two available macroscopically distinct states is at any time t in one of these states, i.e., the dichotomic observable $M(t)$ always produces the value +1 or -1.

2) Stationary: The conditional probability $Q_{ij}(t_1, t_2)$ to find a system in state j at time t_2, if it is in state i at time t_1 only depends on the time difference $(t_2 - t_1)$.

LG-like inequalities can then be formulated as follows [26, 27],

$$\mathbf{K}_- = K(0, 2t) - 2K(0, t) \geq -1, \tag{1}$$

$$\mathbf{K}_+ = K(0, 2t) + 2K(0, t) \geq -1, \tag{2}$$

where $K(t_1, t_2)$ denotes the autocorrelation function defined as $K(t_1, t_2) = \langle M(t_1)M(t_2)\rangle$. This inequalities can be shown to be violated by quantum mechanical unitary dynamics. It should be noted that, in principle, the assumption of stationarity narrows down the class of macrorealist theories which are put to the test. However the stationarity assumption can lead to testable inequalities, on the one hand, and on the other hand, we should stress that it is an assumption that could be tested independently, as opposed for instance to the situation encountered with standard Bell inequalities, where the so called "fair sampling assumption" is not testable [28]. As a result, if the stationarity condition does hold for the consider experimental set up, we argue that the inequalities of the form Eqs.(1,2) provide a fair test for a broad class of macrorrealistic models in that set up.

Here we present an experimental violation of this form of a LGI with macroscopic crystals. The validity of the stationary assumption in this system is experimentally verified with an

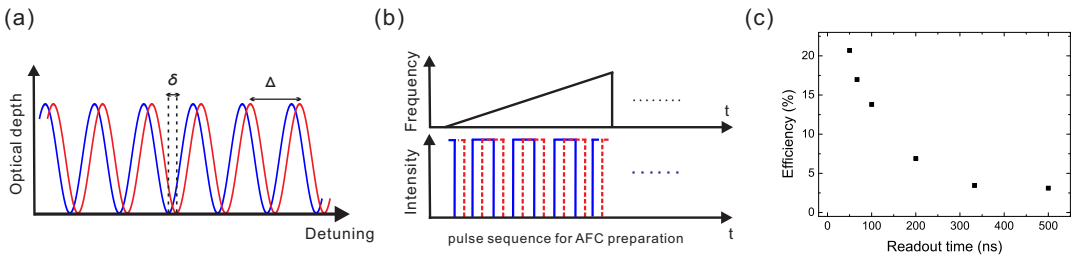

FIG. 1: (a). The H (blue) and V (red) parts of the atomic frequency comb (AFC) are prepared with a periodicity of Δ and a relative detuning of δ. (b). The pulse sequence for AFC preparation used in the experiment. The frequency of pump light are scanned in each cycle while the intensities of H (blue solid line) and V (red dashed line) polarized light are modulated periodically. (c). The readout efficiency at different times.

independent test. The physical system undergoing evolution is composed of about 10^{10} ions, which are spatially distributed into two, 2.4 mm separated crystals. The experimental sample, which was presented in [11] to demonstrate a memory hardware, is composed of two pieces of Nd^{3+}:YVO_4 crystals (doping level 10 ppm) sandwiching a half-wave plate (HWP). The sizes of the two crystals are nearly equal with 1.4 ± 0.01 mm length along the a-axis. The ${}^4I_{9/2} \rightarrow {}^4F_{3/2}$ transition of Nd^{3+} at about 879.705 nm in the Nd^{3+}:YVO_4 crystal shows strong absorption of H polarized photons and little absorption of V polarized photons [29]. Here, $H(V)$ denotes horizontal (vertical), which is defined to be parallel (perpendicular) to the crystal's c-axis. By using a 45° HWP, sandwiched between two parallel Nd^{3+}:YVO_4 crystals, the sample shows nearly equal absorption depth for H and V polarized photons.

We utilize the atomic frequency comb (AFC) technique to realize the reversible transfer of photonic polarization state and atomic state [9–13]. By independently preparing two frequency detuned AFC in the two crystals, we obtained a polarization dependent AFC, which enable us to initialize, control and analyze the collective excitation states of the crystals.

The AFC protocol requires a pumping procedure to tailor the absorption profile of an inhomogeneously broadened solid state atomic medium with a series of periodic and narrow absorbing peaks separated by Δ (see Fig. 1). The single input photon is then collectively absorbed by all the atoms in the comb. The atomic state with and without the photon excitation can be represented by $|e\rangle_N = \sum_j^N c_j e^{-ikz_j} e^{i2\pi\delta_j t} |g_1 \cdots e_j \cdots g_N\rangle$ [9] and $|g\rangle_N =$

$|g_1 \cdots g_j \cdots g_N\rangle$, respectively. Here N is the total number of atoms in the comb; $|g_j\rangle$ and $|e_j\rangle$ represent the ground and excited states, respectively, of atom j; z_j is the position of atom j; k is the wavenumber of the input field; δ_j is the detuning of the atom with respect to the laser frequency and the amplitudes c_j depend on the frequency and on the position of atom j. Due to the periodical structure of AFC, $\delta_j \simeq m_j\Delta$ with m_j of integer. With the two AFC of the two crystals prepared with the same periodicity Δ, when the input photon's polarization is chosen as $H + e^{i\varphi_0}V$, the atomic state of the two crystals will be excited simultaneously, and can be represented by $\Psi(t) = 1/\sqrt{2}(|a\rangle + |b\rangle e^{i(2\pi\delta t+\varphi_0)})$ where $|a\rangle$ and $|b\rangle$ are the excitation states of atoms in the first and second crystals, respectively. δ is the frequency detuning between the two AFC, as shown in Fig. 1(a). The two crystals are actually in an entangled state which can be rewritten as $1/\sqrt{2}(|e\rangle_{N1}|g\rangle_{N2} + |g\rangle_{N1}|e\rangle_{N2}e^{i(2\pi\delta t+\varphi_0)})$. This entanglement has been already demonstrated in a non-polarizing configuration [30].

Now we define the observable $M(t)$ as the superposition state of the collective excitation in the two crystals, where the linear state $|D\rangle = 1/\sqrt{2}(|a\rangle + |b\rangle)$ is used as $|0\rangle$ with eigenvalue equal to +1 and the orthogonal state $|A\rangle = 1/\sqrt{2}(|a\rangle - |b\rangle)$ is used as $|1\rangle$ with eigenvalue equal to -1. In which sense can the states $|D\rangle$ and $|A\rangle$ be branded as 'macroscopically distinct'? Despite both states involve delocalized excitations over a mm scale, attending to the original formulation of Leggett [2, 31], the considered states do not have a sufficiently high degree of *disconnectivity* and therefore their macroscopicity would be arguable. However, and that is a crucial part of our proposal, the two states $|D\rangle$ and $|A\rangle$ differ by a collective phase shared by $\sim 10^{10}$ ions and it is this phase which dictates whether or not the system behaves as a quantum coherent superposition or as a (classical) statistical mixture. We should emphasize that unlike the circulation quantization in superfluid helium or Josephson effect in superconductors, the acquired phase difference between states $|a\rangle$ and $|b\rangle$ cannot be simply interpreted as an accumulated microscopic quantum effect of several ions. Considering the AFC bandwidth $\Gamma_{AFC} = 60$ MHz and the homogeneous linewidth of Nd^{3+} ions $\Gamma_h = 63$ kHz which have been measured under similar experimental conditions [29], we can estimate that at least $\Gamma_{AFC}/\Gamma_h \sim 10^3$ different ions have to contribute to the AFC absorption and the envelope evolutions. The elementary AFC composed of about 10^3 ions just likes a diffraction grating in the frequency domain, which governs the evolution of the atomic coherence and leads to a temporal delayed echo emission. One cannot further divide the elementary AFC grating into single ions to mimic the described evolution

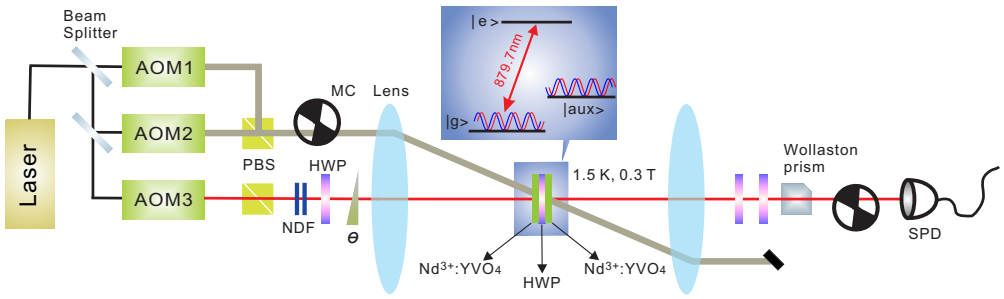

FIG. 2: The experimental setup for violation of LGI with macroscopic crystals. The AOM1 (AOM2) produces V (H) polarized pump light for the AFC preparation. The AOM3 produces a weak probe light for the storage sequence. The probe light's polarizations are controlled by the polarization beam splitters (PBS), the half-wave plate (HWP) and the phase plate (θ). The samples are placed in a cryostat with a temperature of 1.5 K and a magnetic field of 0.3 T. Beyond the sample, a 45° HWP corrects polarization rotation caused by the sample. The probe light's polarizations are then analyzed with HWP and a Wollaston prism. The two MCs are used to protect the single-photon detector (SPD) from classical pump pulses.

in our current experiment. The proposed test therefore goes beyond the demonstration of meso/macroscopic quantum coherence in collective phenomena.

The crystals' state now can be represented by,

$$\Psi(t) = 1/2(1 + e^{i(2\pi\delta t+\varphi_0)})|D\rangle + 1/2(1 - e^{i(2\pi\delta t+\varphi_0)})|A\rangle \tag{3}$$

To probe the crystals' state, we need to collectively transfer the delocalized atomic state into a photon state. Thanks to the periodic structure of AFC, a strong rephasing echo occurs after a time $\tau_s = 1/\Delta$. The photon is re-emitted in the forward direction as a result of a collective interference between all of the atoms that are in phase. The crystal's state $|D\rangle$ and $|A\rangle$ corresponds to readout photon polarization of $H + V$ and $H - V$, respectively.

Fig. 2 shows the experimental setup for investigating the evolution of the macroscopic crystals. The laser source is a cw Ti:sapphire laser (M Squared, Solstis). The H and V polarized pump light is independently generated with two 260 MHz AOM (Brimrose, RF bandwidth: 120 MHz) in double-pass configurations and combined with a polarization beam splitter (PBS). To protect the single-photon detectors (SPD) during the preparation procedure, two phase-locked mechanical choppers (MC) are placed in the pumping optical path and before the SPD, respectively. The H and V polarized pump light are mostly

absorbed by the first crystal and the second crystal, respectively. Carefully adjusting the H and V polarized pump power can optimize the storage efficiency and balance the efficiency of the retrieved H and V components. The photons to be stored are generated by another 260 MHz AOM in double-pass configuration. The probe light are decreased to about 0.5 photons per pulse by the neutral density filters (NDF).

The pump light overlap with the probe light at the sample with a non co-linear configuration. The probe light focuses to a diameter of about 100 μm, while the two pump light is independently collimated to produces a much larger diameter on the sample. The sample is placed in a cryostat (Oxford Instruments, SpectromagPT) at a temperature of 1.5 K and with a superconductor magnetic field of 0.3 T in the horizontal direction. The two parallel Nd^{3+}:YVO_4 crystals' c-axes are placed in the horizontal direction. The probe light's polarization is controlled with a HWP and a phase plate (θ). Because each crystal only strongly absorbs H polarized light, the H polarized input photon is stored in the first crystal, and the V polarized light is stored in the second crystal after polarization rotation by the HWP. To rotate the polarization back to the input state, another HWP is placed at 45° outside of the cryostat. The HWP and Wollaston Prism together choose the polarization of the single photon detections. The signal from the SPD is sent to the time-correlated single photon counting system (Ortec).

The AFC preparation pulse sequence are shown in Fig. 1(b), in which the pump light's frequency is swept over 60 MHz in 240 μs and each frequency step has been assigned a specific amplitude to give an comb structure. The AOM1 and AOM2 are programmed to give two AFC structures with the same periodicity Δ and the frequency detuning of δ. An experimental AFC structure with a periodicity of 20 MHz and δ of 5 MHz is given in the Supplemental Information. The readout efficiency at different evolution time is shown in Fig. 1(c). We note that the AFC created directly in the frequency domain shows a better performance of readout efficiency and requires less laser power consumption.

The pump and probe timing are controlled by two arbitrary function generators (AFG, Tektronix, AFG3252). To avoid the fluorescence noise caused by the classical pumping light, the probe cycle begins after waiting for time $T_w = 1.2\ ms$ after the preparation cycle is completed. During the probe cycle, 1600 weak pulse with temporal width of about 25 ns are sent into the sample with a frequency of 1 MHz. The complete pump and probe cycles are repeated at a frequency of 40 Hz. A digital delay generator (SRS, DG645) provides the

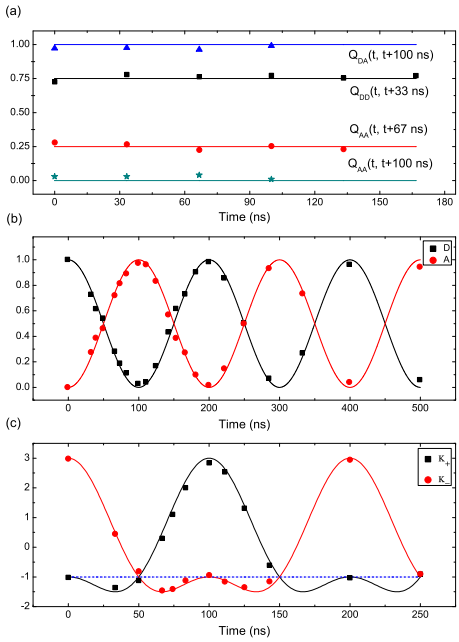

FIG. 3: (a). Experimental test on the validity of stationary assumption. With an AFC prepared with a δ of 5 MHz, the conditional probabilities $Q_{DA}(t, t+100$ ns) (blue triangles), $Q_{DD}(t, t+33$ ns) (black squares), $Q_{AA}(t, t+67$ ns) (red dos) and $Q_{AA}(t, t+100$ ns) (green stars) show little dependence on the evolution time t. The Solid lines are the theoretical predictions. (b). With an AFC prepared with a δ of 5 MHz and the initial state of D, the possibility to find crystals' state in D (black squares) and A(red dots) in different times. (c). The envelope evolution of K_- (black squares) and K_+ (red dots). The Solid lines are the ideal quantum mechanical predictions and the blue dashed line is the classical bound.

trigger signal for coincidence logic of single photon counting.

We first present an experimental test on the validity of stationary assumption in our system. By controlling the probe photon's polarization, we can change the initial state of the crystals and let the crystals' state be D (A) at different readout time t (see methods). Fig. 3(a) shows the conditional probability $Q_{ij}(t, t+\tau)$ to find a system in state j at time $t+\tau$, if it is in state i at time t. It can be seen that $Q_{ij}(t, t+\tau)$ only depend on time difference τ and show little dependence on the evolution time t within experimental errors, thus the stationary assumption holds in our system.

We now analyze the LGI under the classical realistic description, where the two crystals can only be in one of the two states D and A. The input state is initially in $\rho_0 = D$,

after evolution time t, the state becomes statistical mixtures $\rho_t = (1-\alpha)D + \alpha A$, where α represents the influence of the evolution with time t. We can get $K(t) = 1 - 2\alpha$. With further identical evolution time t with the same process, the final state evolves to $\rho_{2t} = (\alpha^2 + (1-\alpha)^2)D + 2\alpha(1-\alpha)A$. Therefore, $Q(2t) = 4\alpha^2 - 4\alpha + 1$. It is easy to verify that $K(2t) - 2K(t) = 4\alpha^2 \geq -1$ and $K(2t) + 2K(t) = 4(\alpha-1)^2 \geq -1$.

Next, we analyzed the experiment from the viewpoint of quantum mechanics. Using Eq.(3) as the specification of our quantum state, we can easily obtain the correlation function $K(t) = \cos(2\pi\delta t)$. With the same analysis, $K(2t) = \cos(4\pi\delta t)$. The functions $K_\pm$ in Eqs.(1,2) can be calculated as $\mathbf{K}_- = \cos(4\pi\delta t) - 2\cos(2\pi\delta t)$ and $\mathbf{K}_+ = \cos(4\pi\delta t) + 2\cos(2\pi\delta t)$. It can be seen that $\mathbf{K}_-$ reaches its minimum value of -1.5 when $2\pi\delta t = \pi/3$ and $\mathbf{K}_+$ reaches its minimum value of -1.5 when $2\pi\delta t = 2\pi/3$, which yields to maximal violation of the inequalities Eq.(1) and Eq.(2), respectively.

Fig. 3(b) shows the corresponding evolution of the crystals' state with an initial state specified by D. With the AFC prepared with δ of 5 MHz, the possibility to find the state D (A) oscillates with a periodicity of 200 ns. Based on the measurement results in Fig. 3(b), the evolution of $\mathbf{K}_-$ and $\mathbf{K}_+$ are shown in Fig. 3(c). The solid lines are theoretical predictions based on Eq. 3. $\mathbf{K}_+$ reaches -1.44 ± 0.06 at 67 ns, which violates the classical limit of -1 by about 7 standard deviations. The value of $\mathbf{K}_-$ at 33 ns has been measured to be -1.34 ± 0.07, which deviates from the theoretical prediction. This is mostly caused by slow response of the AOM, which makes the imperfect separation of the transmitted photons and the readout photons for short storage time.

The user-programmable AFC polarization detuning δ determines the phase evolution speed of the crystals' state. The violation of LGI should hold for a different δ, i.e., a different evolution speed. We further show the envelope evolution of $\mathbf{K}_-$ and $\mathbf{K}_+$ with a δ of 2.5 MHz in Fig. 4. The corresponding crystals' state evolution is shown in Fig. 4(a), it oscillates with a periodicity of 400 ns. $\mathbf{K}_+$ ($\mathbf{K}_-$) reaches -1.45 ± 0.06 (-1.43 ± 0.07) at 67 ns (125 ns), which violates the classical limit of -1 by about 7 standard deviations. We attribute the deviations from the theoretical predictions to the imperfect spatial mode matching of the retrieved H and V components.

The physical system undergoing evolution can be further enlarged by choosing dopants with narrower homogenous linewidth. The figure of merit Γ_{AFC}/Γ_h can be larger than 10^7 since a homogeneous linewidth of 50 Hz have been obtained in Er^{3+}:YSO crystals [32]. In

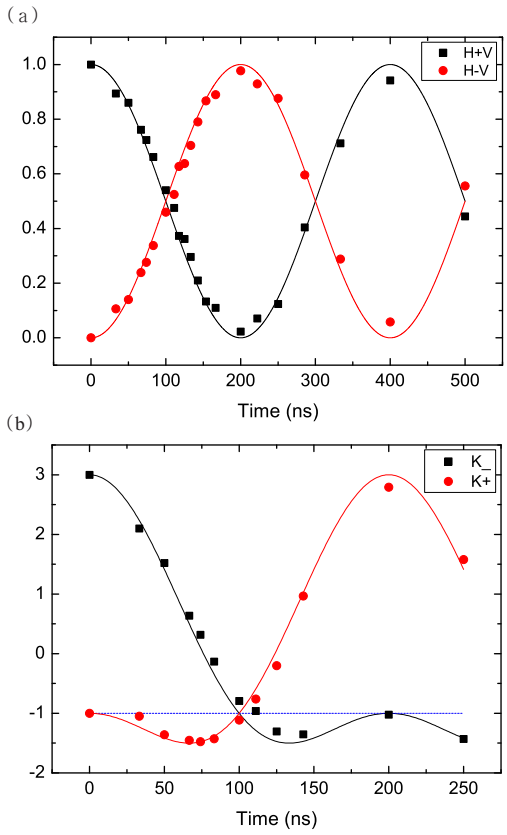

FIG. 4: (a). With an AFC prepared with a δ of 2.5 MHz and the initial state of D, the possibility to find crystals' state in D (black squares) and A(red dots) in different times. (b). The envelope evolution of $\mathbf{K}_-$ (black squares) and $\mathbf{K}_+$ (red dots). The Solid lines are the ideal quantum mechanical predictions and the blue dashed line is the classical bound.

that case more individual ions will contribute to the elementary AFC gratings. The distance between the crystals is not limited to 2.4 mm as obtained in our experiment. Referring to another experimental realization of quantum memory for photonic polarization with similar setup [12], in which the optical distance between two Nd^{3+}:YSO crystals is about 1 m. The high fidelity performance of that quantum memory demonstrates that increasing the distance between two crystals generally do not affect the coherence between them. Thus the two crystals can in principle be brought much further apart in our work.

In summary, we experimentally observed the coherent superposition of delocalized states of macroscopic systems and controlled their evolution with time. These results demonstrate that the dynamics of a collective excitation which is distributed in two macroscopic crystals cannot described by a macrorealistic theory. Contrary to the situation encountered is

collective effects yielding to standard macroscopic quantum coherence, the phase relation between the considered states is governed by a macroscopic number of atoms and therefore the observed *interference* effects are macroscopic in origin although the interfering states themselves are of low Leggett-disconnectivity. Since the stationary assumption was experimentally verified in our system, the violation of this form of LGI represents a strict test against macroscopic realistic models of the described set up. These results confirm the persistence of quantum effects in systems of increasing complexity which can even be seen with naked human eyes.

Methods

Polarization dependent AFC preparation. The AFC preparation pulse sequence are shown in Fig. 1(b), it requires simultaneously sweeping the laser frequency and modulating its intensity. This pumping technique has been used previously in [33]. In our experiment the pump light's frequency is swept over 60 MHz in 240 μs and each frequency step has been assigned a specific amplitude to give an comb structure. This procedure ensures a spectral tailoring resolution of about 500 KHz. The pump sequences are continuously repeated in 10 ms to achieve an optimal AFC structure. The duty ratio in each cycle is carefully adjusted to take into account the power broadening effect. The AOMs are all controlled by programmable RF drivers. The AOM1 and AOM2 are programmed to give a polarization dependent AFC structure with a user controlled frequency detuning of δ. Refer to the experimental AFC structure given in the Supplemental Information, we conclude that the more than twofold efficiency promotion compared to our previous experiment [11] is mainly caused by the unaffected peak absorption of AFC teeth.

Experimental test on the validity of stationary assumption. The input photon's polarization is rotated to $H+V$ $(H-V)$ by the HWP. To detect the crystals' state in D (A) at different readout time t, the probe photon state should be set as $H+e^{i\varphi_0}V$ $(H-e^{i\varphi_0}V)$ with $\varphi_0 = -2\pi\delta t$ by carefully adjusting the phase plate θ. This photon state is directly mapped to the crystals' initial state. The subsequent system evolution is recorded as the function of the time difference τ. The conditional probabilities $Q_{ij}(t, t+\tau)$ only depends on the time difference τ and have little difference for different time t, as shown in Fig. 3(a). These results demonstrate that the stationary assumption is valid in our system.

We are most grateful to A. J. Leggett for his comments on the preliminary version of this manuscript and to C. Brukner for his feedback on the revised version. This work was supported by the National Basic Research Program (2011CB921200), National Natural Science Foundation of China (Grant Nos. 60921091 and 10874162), the EU STREP projects PICC and the EU Integrated Project Q-Essence.

[1] Leggett, A. J. and Garg, A. Quantum mechanics versus macroscopic realism: Is the flux there when nobody looks? *Phys. Rev. Lett.* **5**4, 857 (1985).

[2] Leggett, A. J. Realism and the physical world. *Rep. Prog. Phys.* **7**1, 022001 (2008).

[3] Xu, J. S., Li, C. F. Zou, X. B. and Guo, G. C. Experimental violation of the Leggett-Garg inequality under decoherence. *Scientific Reports* **1**, 101 (2011).

[4] Goggin, M. E. *et al.* Violation of the Leggett-Garg inequality with weak measurements of photons. *Proc. Natl Acad. Sci.* **1**08, 1256 (2011).

[5] Waldherr, G., Neumann, P., Huelga, S. F., Jelezko, F. and Wrachtrup, J. Violation of a temporal Bell inequality for single spins in a diamond defect center. *Phys. Rev. Lett.* **1**07, 090401 (2011).

[6] Dressel, J., Broadbent, C. J., Howell, J. C. and Jordan. A. N. Experimental Violation of Two-Party Leggett-Garg Inequalities with Semiweak Measurements. *Phys. Rev. Lett.* **1**06, 040402 (2011).

[7] Knee, G. C. *et al.* Violation of a Leggett-Garg inequality with ideal non-invasive measurements. *Nature Communications* **3**, 606 (2012).

[8] Palacios-Laloy, A. *et al.* Experimental violation of a Bell's inequality in time with weak measurement. *Nature Physics* **6**, 442 (2010).

[9] Afzelius, M., Simon, C., de Riedmatten, H. and Gisin, N. Multimode quantum memory based on atomic frequency combs. *Phys. Rev. A.* **7**9, 052329 (2009).

[10] de Riedmatten, H., Afzelius, M., Staudt, M. U., Simon, C. and Gisin, N. A solid-state light-matter interface at the single-photon level. *Nature* **4**56, 773 (2008).

[11] Zhou, Z. Q., Lin, W. B., Yang, M., Li, C. F. and Guo, G. C. Realization of reliable solid-state quantum memory for photonic polarization-qubit. *Phys. Rev. Lett.* **1**08, 190505 (2012).

[12] Clausen, C., Bussieres, F., Afzelius, M., Gisin, N. Quantum storage of polarization qubits in

birefringent and anisotropically absorbing materials. *Phys. Rev. Lett.* **1**08, 190503 (2012).

[13] Gündoğan, M., Ledingham, P. M., Almasi, A., Cristiani, M., de Riedmatten, H. Quantum Storage of a Photonic Polarization Qubit in a Solid. *Phys. Rev. Lett.* **1**08, 190504 (2012).

[14] Schrödinger, E. Die gegenwärtige Situation in der Quantenmechanik. *Naturwissenschaften* **2**3, 807, 823, 844 (1935).

[15] Einstein, A., Podolsky, B. and Rosen, N. Can quantum-mechanical description of physical reality be considered complete? *Phys. Rev.* **4**7, 777 (1935).

[16] Bell, J. S. On the Einstein Podolsky Rosen Paradox. *Physics* **1**, 195 (1964).

[17] Aspect, A., Dalibard, J. and Roger, G. Experimental Test of Bell's Inequalities Using Time - Varying Analyzers. *Phys. Rev. Lett.* **4**9, 1804 (1982).

[18] Weihs, G., Jennewein, T., Simon, C., Weinfurter, H. and Zeilinger. A. Violation of Bell's Inequality under Strict Einstein Locality Conditions. *Phys. Rev. Lett.* **8**1, 5039 (1998).

[19] Rowe, M. A., Kielpinski, D., Meyer, V., Sackett, C. A., Itano, W. M., Monroe, C. and Wineland, D. J. Experimental violation of a Bell's inequality with efficient detection. *Nature* **4**09, 791 (2001).

[20] Wilde M. M, McCracken J. M and Mizel A. Could light harvesting complexes exhibit non-classical effects at room temperature? *P*roceedings of the Royal Society A **466** 1347 (2010).

[21] Fleming G. R., Huelga, S. F. and Plenio, M. B. Focus on quantum effects and noise in biomolecules New J. Phys. **13** 115002 (2011)

[22] Ghirardi, G. C., Rimini, A. and Weber, T. Unified dynamics for microscopic and macroscopic systems. *Phys. Rev. D.* **3**4, 470 (1986).

[23] Ghirardi, G. C., Pearle, P. and Rimini, A. Markov processes in Hilbert space and continuous spontaneous localization of systems of identical particles. *Phys. Rev. A*. **4**2, 78 (1990).

[24] Bassi, A., and Ghirardi, G. Dynamical reduction models. *Physics Reports* **3**79, 257 (2003)

[25] Penrose, R. Gravity's role in Quantum State Reduction. *Gen. Relativ. Grav.* **2**8, 581 (1996).

[26] Huelga, S. F., Marshall, T. W. and Santos, E. Proposed test for realist theories using Rydberg atoms coupled to a high-Q resonator. *Phys. Rev. A*. **5**2, R2497 (1995).

[27] Huelga, S. F., Marshall, T. W. and Santos, E. Temporal Bell-type inequalities for two-level Rydberg atoms coupled to a high-Q resonator. *Phys. Rev. A.* **5**4, 1798 (1996).

[28] Clauser, J. F. and Shimony, A. Bell's theorem. Experimental tests and implications. *Rep. Prog. Phys.* **4**1, 1881 (1978).

[29] Hastings-Simon, S. R., Afzelius, M., Minář, J., Staudt, M. U., Lauritzen, B., de Riedmatten, H. and Gisin, N. Spectral hole-burning spectroscopy in Nd^{3+}:YVO_4. *Phys. Rev. B.* **77**, 125111 (2008).

[30] Usmani, I. *et al.* Heralded quantum entanglement between two crystals *Nature Photonics* **6**, 234 (2012).

[31] Leggett, A. J. Macroscopic quantum systems and the quantum theory of measurement. *Prog. Theor. Phys. Supplement* **6**9, 80 (1980).

[32] Sun, Y. *et al.* Recent progress in developing new rare earth materials for hole burning and coherent transient applications. *Journal of Luminescence* **9**8, 281 (2002).

[33] Lauritzen, B. *et al.* Telecommunication-wavelength solid-state quantum memory at the single photon level. *Phys. Rev. Lett.* **1**04, 080502 (2010).

Supplementary Information

Polarization dependent AFC structure

In our experiment, an optimized efficiency of about 21% at 50 ns storage time is obtained. We measure the AFC structure by sending long probe pulse and measuring their transmission. An example AFC, with a periodicity of 20 MHz and δ of 5 MHz, is shown in the Fig. S1. Compared with our previous paper, the efficiency promotion is mainly caused by the large available optical depth (~ 6.2). The peak absorption is preserved because the inhomogeneous absorption is directly tailored in frequency domain. The experimental efficiency fits well the theoretical estimation. For longer storage time, the readout efficiency drops because of a rising background absorption.

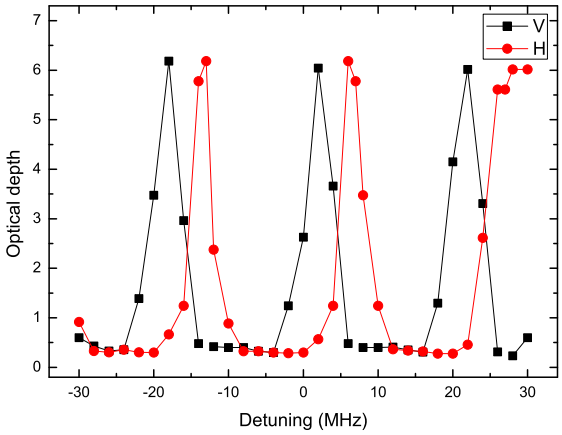

FIG. 5: An AFC prepared with a periodicity of 20 MHz and δ of 5 MHz. The red circles are measured with H polarized probe light and the black squares are measured with V polarized probe light.